

Frozen-in correlations in $K_{1-x}(NH_4)_xI$ mixed crystals: A Raman-scattering study

Jean-François Berret and Jean-Louis Sauvajol

Groupe de Dynamique des Phases Condensées, Université de Montpellier II, F-34095 Montpellier, France

(Received 6 December 1993)

We report on low-frequency Raman-scattering results obtained on $K_{1-x}(NH_4)_xI$ mixed crystals and on its deuterated isomorph ($x=0.46$ and 0.62) as a function of temperature. With decreasing temperature, the Raman susceptibility is dominated by the growth and the narrowing of a strong component around 30 cm^{-1} and a much weaker one at 44 cm^{-1} . A comparison of the present results with recent inelastic neutron scattering data on the same mixed crystals enabled us to assign the components at 30 and 44 cm^{-1} to the density of states of transverse and longitudinal acoustic phonons at the Brillouin-zone boundary. For the most prominent band, it is also shown that the drastic increase of the intensity coincides with the onset of freezing of antiferroelectric correlations evidenced by diffuse scattering measurements ($T_F=45$ and 58 K for $x=46\%$ and 62% , respectively). The strong activity of the zone-boundary acoustic branches below T_F is interpreted in terms of breaking of the local symmetry of the mixed crystal. Finally, the temperature dependences of the main Raman active components identified below 250 cm^{-1} are also discussed, with particular attention to aspects relevant to the freezing transition and to the orientational disorder.

I. INTRODUCTION

During the last decade, intense theoretical and experimental investigations on mixed molecular crystals have shown the existence of two new classes of glasses: the electric and elastic orientational glasses (OG). Prototype systems are the ferro-antiferroelectric mixtures $Rb_{1-x}(NH_4)_xH_2PO_4$ and the mixed cyanide crystals $(KBr)_{1-x}(KCN)_x$, respectively. An extensive review has been devoted to orientational glasses recently.¹ One of the most appealing properties of OG's is the freezing process of the orientational degrees of freedom which occurs as temperature is lowered. The slowing-down of the molecular dynamics shows strong resemblances with the transitions in magnetic spin and structural glasses.

Owing to the importance of OG's for the understanding of glass formation, new systems with orientational disorder are highly needed. Recently, the ammonium-potassium iodide crystals, $K_{1-x}(NH_4)_xI$ and its deuterated isomorph have attracted much attention because this mixed crystal exhibits an orientational glassy phase at low temperature ($T < 50\text{ K}$) and intermediate compositions, $x \sim 0.5$.²⁻⁹ In the earliest reports on this mixed compound, the orientational degrees of freedom have been recognized to be of electric dipolar nature and most likely related to the ammonium ions. In order to explain the value of 1.4 Debye for the electric dipole, two hypothesis have been proposed: The ammonium tetrahedra are distorted by the interactions with the lattice via a crystal field of symmetry C_{3v} ,^{2,3} or the NH_4 occupy off-center positions out of the lattice sites.⁴

At room temperature, the $K_{1-x}(NH_4)_xI$ compounds exhibit a rocksalt structure, where the ammonium tetrahedra are orientationally disordered. Typical reorientation times have been estimated to some picoseconds.¹⁰ A schematic (x, T) phase diagram has been derived recently by the combination of x-ray, Raman,

and neutron-scattering measurements.⁷ It is illustrated in Fig. 1. On the NH_4 rich side, the mixed system undergoes a structural transition from NaCl to CsCl cubic structures (shown as full lines in Fig. 1). Strong hysteresis effects have been also reported for this first-order transition which is believed, moreover, to have a Martensitic character. Until a critical concentration x_c is reached ($x_c \sim 0.75$), the substitution $K \rightarrow NH_4$ shifts the transitions to lower temperatures. Below x_c , no phase transition occurs and the crystals with $x \geq 0.3$ enter an orientational glass state devoid of long-range orientational order. This orientationally disordered state has been evidenced by means of dielectric spectroscopy⁴ and coherent neutron scattering.⁵ The latter experiments have shown in addition the growth of antiferroelectric

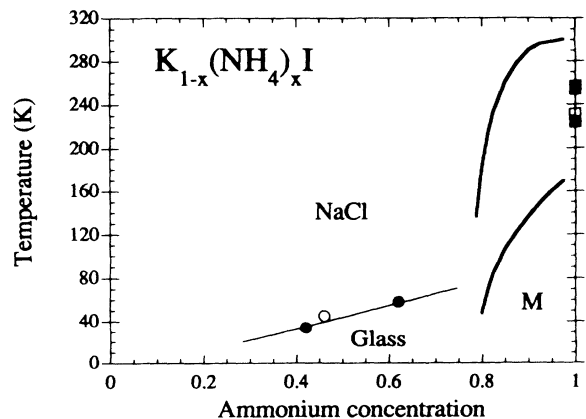


FIG. 1. Schematic (x, T) phase diagram of $K_{1-x}(NH_4)_xI$ mixed crystals as proposed in Ref. 7. Full symbols refer to deuterated compounds. The two concentrations investigated here by Raman scattering, $x=0.46$ and $x(D)=0.62$ are in the orientational glassy range.

frozen-in correlations below the freezing temperature T_F (shown by the straight line in Fig. 1).

In this paper we investigate the low-frequency Raman responses of $K_{1-x}(NH_4)_xI$ mixed crystals ($\nu < 250 \text{ cm}^{-1}$) in the temperature range $T = 15\text{--}300 \text{ K}$. Two single crystals with ammonium concentrations $x = 0.46$ and $x(D) = 0.62$ have been studied, the second sample being fully deuterated (as indicated by the D in parenthesis). In order to probe the freezing process, we had to take advantage of two properties: First, orientational disorder in plastic crystals is known to destroy the wave-vector conservation rule of Raman light-scattering processes ($q \sim 0$). Thus, phonons of the whole Brillouin zone which feel this disorder can contribute to the Raman response. The second property is the coupling of the zone-boundary transverse acoustic (TA) mode with NH_4 reorientations.⁵ This coupling was established directly by neutron measurements. The TA dispersion curve at the X point (i.e., for reduced wave vector $q^* \sim 1$ propagating in the $[001]$ direction) was shown to soften with decreasing temperature.

The former feature, that is the contribution of the phonon density of states to the light scattered spectrum, was the topic of our first Raman report on $K_{1-x}(NH_4)_xI$ (hereafter referred to as I).¹¹ By comparing the data from the paraelectric regime and from the orientational glassy phase for different ammonium contents ($x = 0.005\text{--}0.46$), five translational and two rotational components could be identified below 250 cm^{-1} . In this paper, we focus our attention only on the Raman-active components which are sensitive to the freezing transition in these mixed crystals.

II. EXPERIMENTAL DETAILS AND RESULTS

Both $K_{0.54}(NH_4)_{0.46}I$ and $K_{0.38}(ND_4)_{0.62}I$ single crystals were grown from aqueous solutions by Haussühl at the Universität zu Köln. The samples arise from the same batch than the ones studied previously by means of Brillouin³ and neutron^{7,8} scattering. As in I, freshly cleaved monocrystals were placed in a helium cryostat on the Ar^+ laser beam in a 90° configuration ($\lambda_0 = 5145 \text{ \AA}$). Stokes and anti-Stokes spectra were collected in a single run by scanning over the $-80\text{--}250 \text{ cm}^{-1}$ region. The two polarizations labeled $[x(zz)y]$ and $[x(zx)y]$ have been investigated. Here $x = \langle 100 \rangle$ and $y = \langle 010 \rangle$ define the axes for incident and scattered light, respectively. The local temperature of the scattering volume was determined from the Stokes and anti-Stokes intensity ratios of several low-frequency bands and using the Boltzmann statistics. Typical deviations between the imposed and the true temperatures are usually of the order of 10 K . The accurate measurement of the crystal temperature is of particular importance in the determination of the freezing temperature T_F .

All spectra shown in the following (in contrast to I) are plotted in terms of Raman susceptibility $\chi''(\nu, T)$, which is obtained by dividing the scattered intensity $I(\nu, T)$ by the Bose-Einstein factor with T derived from the previous procedure:

$$\chi''(\nu, T) \propto I(\nu, T) [1 - \exp(-h\nu/k_B T)]^{-1}$$

In Figs. 2 and 3 are shown the temperature evolution of Raman spectra in $K_{0.54}(NH_4)_{0.46}I$ and $K_{0.38}(ND_4)_{0.62}I$ for the $x(zz)y$ polarization. It corresponds to Raman-allowed transition of symmetry $A_{1g} + 4E_g$. The Raman responses obtained for $T = 15\text{--}135 \text{ K}$ have been shifted with respect to the each other. In Fig. 3, the Stokes side of the $\chi''(\nu, T)$ spectra ($\nu > -80 \text{ cm}^{-1}$) has been included in order to illustrate the procedure explained above. In Figs. 4 and 5 are displayed the susceptibilities in the $x(zx)y$ polarization (T_{2g} modes) for the same two samples ($T = 15\text{--}80 \text{ K}$). The full lines through the data points in the range $10\text{--}80 \text{ cm}^{-1}$ are explained below.

As already emphasized in I, the components contributing to the $A_{1g} + 4E_g$ susceptibility (Figs. 2 and 3) show up at the same frequency but with different intensities in the T_{2g} polarization. Actually, nine Raman-active components have been reported in I for the $K_{1-x}(NH_4)_xI$ mixed compounds up to 600 cm^{-1} . Those of interest for the present work and which will be discussed in detail in the following are indicated by arrows in Figs. 2 and 3 and labeled ν_1 to ν_5 (note that the indexing is now different to that of I). ν_1 to ν_4 are located below 80 cm^{-1} whereas ν_5 around 150 cm^{-1} will be considered only as a comparison (see Table I for the exact low-temperature values of these frequencies).

The most noticeable result of the $\chi''(\nu)$ spectra of Figs. 2–5 is the growth of the strong component around 28 cm^{-1} observed as temperature is lowered. This feature, although present in both samples and polarizations is at best evidenced in the T_{2g} data for $x(D) = 0.62$ (Fig. 5). Note in the same figure the emergence of the weaker component ν_2 at 45 cm^{-1} , which is only clearly experienced at low temperature ($T < 50 \text{ K}$). In the following section, we demonstrate that these features are connected to the freezing in $K_{1-x}(N(H,D)_4)_4I$.

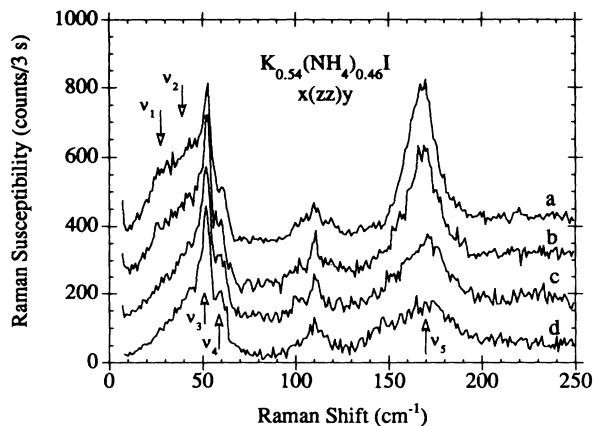


FIG. 2. Temperature evolution of the low-frequency Raman susceptibilities measured in $K_{0.54}(NH_4)_{0.46}I$ for the $x(zz)y$ polarization ($A_{1g} + 4E_g$ symmetry) at temperatures (a) 15 K , (b) 32 K , (c) 56 K , and (d) 87 K . For sake of clarity, each spectrum has been shifted with respect to each other. The Raman-active components studied in the present work are indicated by arrows.

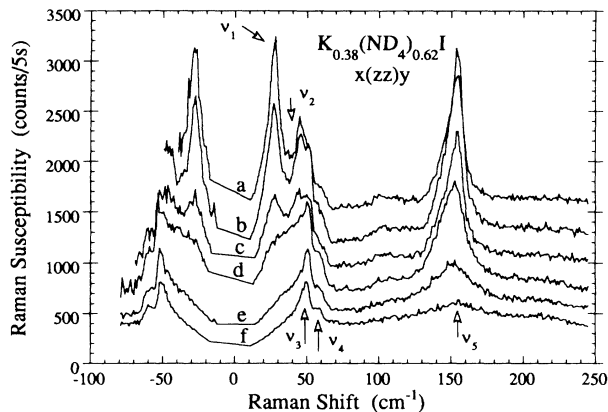


FIG. 3. As in Fig. 2, but for the $K_{0.38}(ND_4)_{0.62}I$ mixed crystal. The temperatures are (a) 14 K; (b) 27 K; (c) 37 K; (d) 53 K; (e) 60 K, and (f) 135 K.

III. ANALYSIS AND DISCUSSION

According to I, the assignment of the five Raman-active components considered here is the following:

(i) Below 80 cm^{-1} , the $A_{1g} + 4E_g$ and T_{2g} spectra are essentially due to the density of states of acoustic phonons. A precise attribution of each mode has been made possible by comparing the low-frequency band shape below 80 cm^{-1} obtained in a deuterated sample $K_{0.58}(ND_4)_{0.42}I$ with the energies of acoustic phonons measured by inelastic neutron scattering in the same crystal.⁵ We thus can assign ν_1 and ν_2 to transverse and longitudinal phonons, respectively propagating in the [001] crystallographic direction at the Brillouin-zone boundary. ν_{TA} values determined for the deuterated crystals are also listed in Table I for comparison. ν_3 is associated to transverse branch in the [011] direction whereas ν_4

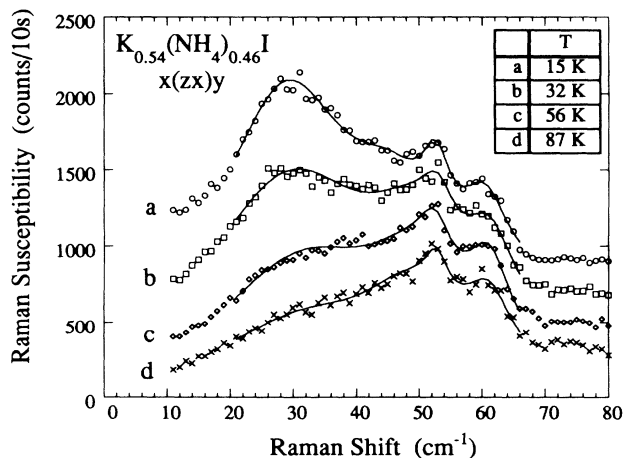


FIG. 4. Low-frequency Raman susceptibilities of $K_{0.54}(NH_4)_{0.46}I$ measured in the $x(zx)y$ polarization (T_{2g} symmetry) at the same temperatures as in Fig. 2. The continuous lines through the data points are results of best-fit calculations using for each component a harmonic oscillator description (see text).

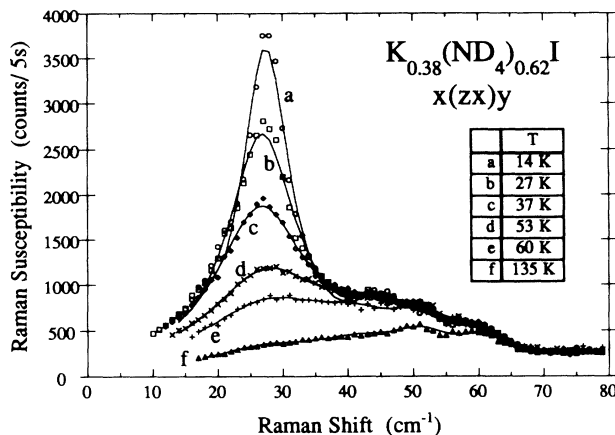


FIG. 5. As in Fig. 4, but for the $K_{0.38}(ND_4)_{0.62}I$ mixed crystal.

arises from the longitudinal phonons traveling along the [001] axis.

(ii) ν_5 has been interpreted in terms of an optical (impurity) mode related to the substitution of ammonium ions in KI. This assignment was based on the calculation of the value of the frequency ratio $\nu_5(NH_4)/\nu_5(ND_4)$ between a protonated and a deuterated crystal at comparable x . As shown in Table I for the ν_5 values at $x(D)=0.42$ and $x=0.46$, it was found to be 1.10, as expected from the mass ratio between deuterated and protonated ammonium ions.

In order to determine accurately the frequency ν_k , the full width at half maximum (FWHM) Γ_k and the intensity I_k of each k component of the low-frequency band shape ($k=1-4$), best-fit calculations of the Raman T_{2g} susceptibilities were performed using damped harmonic oscillators. Since the lines ν_3 and ν_4 are less prominent in this polarization, the analysis was systematically performed on the $x(zx)y$ spectra. It was nevertheless

TABLE I. Compilation of the frequencies (at $\sim 15\text{ K}$) of the Raman-active components investigated here in $K_{1-x}(NH_4)_xI$ mixed crystals and deuterated isomorphs. Since the Raman activity of the modes sensitive to the freezing, ν_1 and ν_2 strongly varies with respect to the concentration, the ν_2 component could not be observed for the deuterated sample at $x(D)=0.42$ ("n.o." stands for "not observed"). ν_{TA} denotes the frequency of the zone-boundary phonon in the [001] direction measured using inelastic neutron scattering (Refs. 5 and 15). The freezing temperatures T_F as received from Fig. 9 are also included for the three systems under interest.

	$x(D)=0.42$	$x(H)=0.46$	$x(D)=0.62$
ν_1 (cm^{-1})	29	28.5	28
ν_{TA} (cm^{-1})	26	n.o.	25
ν_2 (cm^{-1})	n.o.	46	45
ν_3 (cm^{-1})	52	53	51
ν_4 (cm^{-1})	61	61	61
ν_5 (cm^{-1})	153	169	154
T_F (K)	34	45	58

checked that best-fit calculations on the $A_{1g} + 4E_g$ susceptibilities provide comparable results. As indicated by the continuous lines in Figs. 4 and 5, this phenomenological description was found to be appropriate for both concentrations. Results of the fitting procedure performed at $x(D)=0.62$ are shown in Figs. 6, 7, and 8 for the intensity, the frequency and the FWHM, respectively.

The behavior of the first component ν_1 around 28 cm^{-1} is clearly anomalous compared to the other lines: Below $\sim 60 \text{ K}$, its intensity increases drastically, its frequency slightly softens and its FWHM decreases within a factor 3 between 150 and 15 K. The ν_2 component exhibits analogous features, but the changes observed at $\sim 60 \text{ K}$ cannot be considered as significant. Contrary to this, the lines ν_3 and ν_4 remain unchanged over the whole temperature range (Fig. 7). The data for the intensity and FWHM of the ν_5 component have been also included in Figs. 6 and 8 for comparison. As T is lowered, the growth and the narrowing of this optical mode at 150 cm^{-1} occur continuously. No anomalous behavior can be evidenced in the vicinity of the freezing.

Similar qualitative results for the ν_1 and ν_5 modes are obtained for the $x=0.46$ crystal. The temperature variation of the Raman activity for these modes is however less important than that of the $x(D)=0.62$.

We now demonstrate that the occurrence of a strong Raman-active component around 28 cm^{-1} observed with decreasing temperatures for intermediate compositions only ($x=0.4-0.6$), is related to the freezing of the short-range antiferroelectric correlations evidenced by neutron^{5,7} and x-ray experiments.⁸ In Fig. 9 are displayed the temperature dependence of the diffuse neutron intensities observed for the wave vector $Q=(4,1,0)$ in $K_{0.58}(ND_4)_{0.42}I$ and for $Q=(2,1,0)$ in $K_{0.38}(ND_4)_{0.62}I$. They are shown as continuous lines and compared with the $I_1(T)$ data received from Raman spectroscopy performed on the $x=0.46$ and $x(D)=0.62$ samples. For this latter compound (Fig. 9), the onset of freezing characterized by the growth of both intensities occurs at the same temperature $T_F=58 \pm 2 \text{ K}$ (indicated by an arrow). The agreement between the T_F values is consistent with the fact that the Raman and the neutron experi-

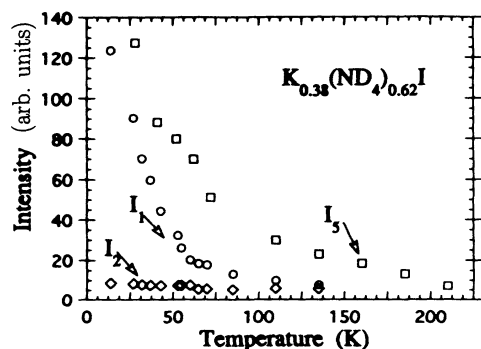


FIG. 6. Temperature dependences of the intensities for the lines ν_1 , ν_2 , and ν_5 , as received from the analysis of the T_{2g} spectra of $K_{0.38}(ND_4)_{0.62}I$. Note the strong increase of $I_1(T)$ below $\sim 60 \text{ K}$.

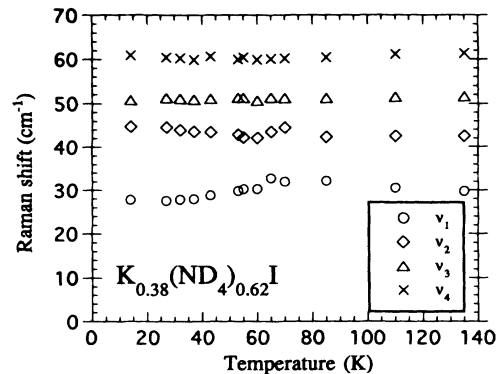


FIG. 7. Temperature variations of the frequencies $\nu_1-\nu_4$ for the Raman-active components showing up below 80 cm^{-1} in $K_{0.38}(ND_4)_{0.62}I$. Note again the decrease of $\nu_1(T)$ below $\sim 60 \text{ K}$.

ments probe the freezing processes at comparable time scale, namely in the picosecond time range. For the $x=0.46$ crystal, however, the Raman data available allows only a rough estimate for the freezing temperature: $T_F(x=0.46) \sim 45 \text{ K}$. The T_F values for the three samples shown in Fig. 9 are listed in Table I.¹² They are also utilized in Fig. 1 to delimit the glassy range of the (x, T) phase diagram.

A second piece of evidence, although more qualitative, of the relationship between the freezing transition and the growth of the ν_1 component with decreasing temperature can be found in Fig. 7. A very careful inelastic neutron study on a $x(D)=0.42$ deuterated isomorph has recently shown that the phonon energy of the transverse-acoustic branch at the zone boundary (in the direction $[001]$) softens with decreasing temperature. It passes then through a minimum around 100 K and recovers at low temperature. Although the determination of the mode frequency by Raman spectroscopy is not accurate (particularly when one remembers that the lines $\nu_1-\nu_4$

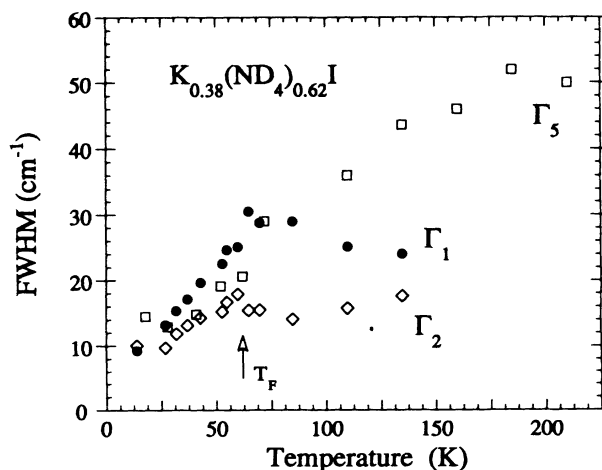


FIG. 8. Full width at half maximum for the components ν_1 , ν_2 , and ν_5 as function of temperature as deduced from the $T_{2g}-\chi''(\omega, T)$ spectra of $K_{0.38}(ND_4)_{0.62}I$.

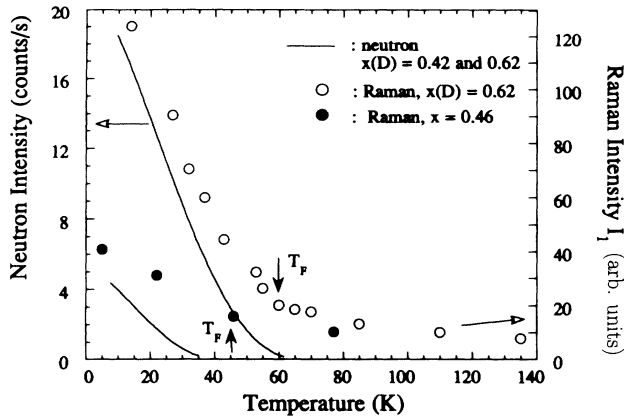


FIG. 9. Temperature dependences of the intensity I_1 related to the low-frequency Raman-active model at 28 cm^{-1} compared to the diffuse scattering signals received from elastic neutron scattering at the Brillouin-zone boundary. On the right scale are displayed the Raman data for $x=0.46$ (closed circles) and $x(D)=0.62$ (open circles). On the left scale the continuous lines refer to elastic neutron data obtained for $x(D)=0.42$ (lower curve) and $x(D)=0.62$ (upper curve) (Ref. 8). The arrows indicate the freezing transition temperatures as deduced from the Raman results.

are due to phonon densities of states), a decrease of the frequency shift ν_1 is nevertheless observed in Fig. 7.

The above Raman results can be interpreted in the light of the already mentioned elastic neutron and x-ray-diffraction data.⁸ As the temperature of a $\text{K}_{1-x}(\text{N}(\text{H},\text{D})_4)_x\text{I}$ sample ($x \sim 0.5$) is lowered, diffuse scattering shows up at the Brillouin-zone boundary (X point). These diffuse peaks have been found to exhibit cigar-shaped contours, indicating strong correlations along the C_4 axis and much weaker ones in the perpendicular direction. These results, observed at low temperatures in both x-ray and neutron experiments are clear indications of local symmetry breaking. More precisely, the local symmetry of the crystal is not any more face-centered cubic, as in the paraelectric regime. The structure is then characterized by a doubling of the lattice cell.

Moreover, the range over which this local ordering takes place has been deduced from the wave-vector dependence of the diffuse scattering. Below T_F , antiferroelectric clusters with typical sizes ξ are building up. For the $x(D)=0.62$ crystal, the correlation length ξ saturates at low temperatures at about 10 lattice cells, that is nearly 60 \AA .⁸ These findings suggest that the TA and LA phonons measured at the zone boundary in the fcc structure are becoming zone-center optical phonons for the low-temperature local symmetry. The Raman activity of these two acoustic branches associated with the ν_1 and ν_2 modes, respectively, is thus clearly enhanced below the freezing. The change of local symmetry with reduced temperature accounts well for the anomalous behaviors evidenced in the intensity, FWHM, and frequency of the ν_1 component (Figs. 6–8, respectively).

Although the band ν_5 exhibits no anomalous behavior at T_F , its temperature variation deserves some comments.

This mode was first observed (at $\nu=224 \text{ cm}^{-1}$) using inelastic neutron scattering in a low-concentrated $\text{K}_{1-x}(\text{NH}_4)_x\text{Cl}$ crystal ($x=7\%$) by Smith, Wakabayashi, and Nicklow,¹³ that is, in a system where no freezing transition is expected to occur. In very good agreement with the ν_5 data of Figs. 6 and 8 however, it was found out that, as the temperature is lowered, the intensity of this mode increases continuously and its width becomes very narrow. Such a T behavior is typical for localized vibrational impurity modes.¹⁴ For the $\text{K}_{1-x}(\text{NH}_4)_x\text{I}$ mixed crystal, it reflects the strong anharmonicity of the crystalline potential felt by the ammonium. Since this band is related to the localized translational motions of the ammonium, one should expect the ν_5 band to be sensitive to the freezing transition, at least in the case of electric dipoles originating from off-center positions of the NH_4 with respect to the lattice site. The temperature variation displayed in Figs. 6 and 8 probably rules out the assumption of dipolar degrees of freedom connected to NH_4 translational motions.

IV. CONCLUSION

The present Raman results associated to those reported in I (Ref. 11) cover the concentration range $x=0.5$ – 62% . As temperature is decreased, the low-frequency Raman scattering of $\text{K}_{1-x}(\text{N}(\text{H},\text{D})_4)_x\text{I}$ mixed crystals is dominated by the growth and the narrowing of a strong component in the 30-cm^{-1} range. This mode has been clearly detected for $x=0.42$, 0.46 , and $x(D)=0.62$, but not at lower concentrations. It should be pointed out that deuteration seems to play a minor role in these systems.

A comparison of the Raman results with inelastic neutron-scattering data on the same compounds first enabled us to assign the band at 30 cm^{-1} as arising from transverse-acoustic branch at the Brillouin-zone boundary. Secondly, we demonstrated that the temperature dependence of this band is correlated with the increase of frozen-in correlations of antiferroelectric type. The intensities of the low-frequency band and that of the diffuse patterns seen by neutron follow comparable behaviors below the freezing temperature T_F . The fact that the Raman response probes the freezing process in these mixed compounds allows us to derive a precise (x, T) phase diagram for $\text{K}_{1-x}(\text{N}(\text{H},\text{D})_4)_x\text{I}$.

Finally, it is worth noting that in none of the above results we clearly infer that the orientational degrees of freedom are strictly dipolar, as originally believed. It has been recently suggested⁸ that static displacements of one or several atoms away from the lattice sites (and most probably the iodide ions) are involved in the freezing. Indeed the electric dipolar nature still remains an open question.

ACKNOWLEDGMENT

Groupe de Dynamique des Phases Condensées is Unité de Recherche Associée au CNRS No. 233.

- ¹U. Höchli, A. Loidl, and K. Knorr, *Adv. Phys.* **39**, 405 (1990).
- ²C. Bostoen, G. Coddens, and W. Wegener, *J. Chem. Phys.* **91**, 6337 (1989). Claude Bostoen, Ph.D. thesis, University of Antwerpen, 1991.
- ³J.-F. Berret, F. Bruchhäuser, R. Feile, C. Bostoen, and S. Haussühl, *Solid State Commun.* **74**, 1041 (1990).
- ⁴I. Fehst, R. Böhmer, W. Ott, A. Loidl, S. Haussühl, and C. Bostoen, *Phys. Rev. Lett.* **64**, 3139 (1990).
- ⁵J.-F. Berret, C. Bostoen, J.-L. Sauvajol, B. Hennion, and S. Haussühl, *Europhys. Lett.* **16**, 91 (1991); J.-F. Berret, J.-L. Sauvajol, and B. Hennion, *J. Phys. Condens. Matter* **4**, 9235 (1992).
- ⁶R. Mukhopadhyay, J. Tomkinson, and C. J. Carlile, *Europhys. Lett.* **17**, 201 (1992).
- ⁷J.-F. Berret, C. Bostoen, and B. Hennion, *Phys. Rev. B* **46**, 13 747 (1992).
- ⁸J.-F. Berret, S. Ravy, and B. Hennion, *J. Phys. I (France)* **3**, 1031 (1993).
- ⁹R. Böhmer, F. Fujara, G. Hinze, and S. Haussühl (unpublished).
- ¹⁰P. S. Goyal and B. A. Dasannacharya, *J. Phys. C* **12**, 209 (1979); **12**, 218 (1979).
- ¹¹J.-F. Berret, J. L. Sauvajol, and S. Haussühl, *J. Chem. Phys.* **92**, 4896 (1992).
- ¹²These T_F values are slightly different from those reported in Ref. 7. This is due to the accurate analysis of the $\chi''(\omega, T)$ spectra performed in the present paper.
- ¹³H. G. Smith, N. Wakabayashi, and R. N. Nicklow (unpublished).
- ¹⁴R. J. Elliott, W. Hayes, G. D. Jones, H. F. Macdonald, and C. T. Sennett, *Proc. R. Soc. London Ser. A* **289**, 1 (1965).
- ¹⁵B. Hennion (private communication).